AIAA JOURNAL
Vol. 31, No. 2, February 1993

Probabilistic Nonlinear Finite Element Analysis of Composite Structures

S. P. Engelstad* and J. N. Reddy†
Virginia Polytechnic Institute and State University, Blacksburg, Virginia 24061

A probabilistic finite element analysis procedure for laminated composite shells is developed. A total Lagrangian finite element formulation, employing a degenerated three-dimensional laminated composite shell element with the full Green-Lagrange strains and first-order shear deformable kinematics, is used. The first-order second-moment technique for probabilistic finite element analysis of random fields is employed, and results are presented in the form of mean and variance of the structural response. Reliability calculations are made by using the first-order reliability method combined with sensitivity derivatives from the finite element analysis. Both ply-level and micromechanics-level random variables are incorporated, the latter by means of the Aboudi micromechanics model. Two sample problems are solved to verify the accuracy of the procedures developed and to quantify the variability of certain material type/structure combinations. In general, the procedure is quite effective in determining the response statistics and reliability for linear and geometric nonlinear behavior of laminated composite shells.

Introduction

THE use of fiber-reinforced composite materials in modern engineering structural design has become a common practice. For example, organic matrix composite materials such as graphite-epoxy have been used extensively with substantial weight savings along with additional benefits such as dimensional stability. However, since more design variables typically exist when composite materials are employed and the manufacturing processes for producing composites are more complex, more variability can exist in a design produced with composites compared to conventional materials. This increased tendency for variability can induce a trend toward design conservatism. Thus, the motivation of this paper is to utilize the probabilistic finite element technique to quantify the variability in composite structures.

Several authors have developed probabilistic finite element methods for random fields or variables. Among the common methods used for nonlinear analysis is the second moment method, as outlined by Hisada and Nakagiri,[1] Nakagiri et al.,[2] Tani and Nakagiri,[3] and Liu et al.[4-6] Nakagiri and co-workers applied the method to the analysis of linear composite plates using classical lamination theory. Liu and his co-workers have done extensive work applying the method to geometric and material nonlinear analysis, but only for isotropic materials.

This paper focuses on the application of the second-moment method to probabilistic finite element analysis of geometric nonlinear composite shells. The procedures developed by Liu et al.[4-6] for determining first-order mean and variance of the deflection, strain, and stress response are utilized. The sensitivity derivatives computed in the second-moment method are also used to perform the first-order reliability optimization. It is of interest to analyze more realistic laminated composite structures; thus, the shell element with shear deformation theory is used in the present study. This paper investigates the computational difficulties in analyzing actual laminated composite panels involving models with large numbers of layers and degrees of freedom and also those that proceed deep into the postbuckling range. A micromechanics theory is included to allow random variables to be formulated at the micromechanics level. Probabilistic sensitivity studies are performed, and comparisons are made with experimental results.

Received April 10, 1991; revision received June 16, 1992; accepted for publication June 16, 1992.

*Assistant Professor, Department of Engineering Science and Mechanics; currently at Lockheed Aeronautical Systems Co., Dept. 73-47, Zone 0685, Marietta, GA 30063.

†Clifton C. Garvin Professor, Department of Engineering Science and Mechanics; currently, Oscar S. Wyatt Chair, Department of Mechanical Engineering, Texas A&M University, College Station, TX 77843.

Finite Element Formulation

The incremental equations of a continuous medium are formulated based on the principle of virtual displacements and the total Lagrangian description. The detailed description can be found in Ref. 7 and is thus omitted here for brevity. The final incremental equilibrium equations for an element are given by

$$([K_L] + [K_{NL}])\{\Delta^e\} = \{R\} - \{F\} \tag{1}$$

where $\{\Delta^e\}$ is the vector of nodal incremental displacements in an element, and $[K_L]$, $[K_{NL}]$, and $\{F\}$ are defined by

$$[K_L] = \int_V [B_L]^T[C][B_L]\,dV$$

$$[K_{NL}] = \int_V [B_{NL}][C][B_{NL}]\,dV$$

$$\{F\} = \int_V [B_L]\{\hat{S}\}\,dV$$

In the preceding equations, $[B_L]$ and $[B_{NL}]$ are linear and nonlinear strain-displacement transformation matrices, $[C]$ is the incremental stress-strain material property matrix, $\{\hat{S}\}$ is a vector of second Piola-Kirchhoff stresses, and $\{R\}$ is the external load vector. All matrix elements refer to the deformed state with respect to the original undeformed configuration. After assembly, the Newton-Raphson method is employed to solve the nonlinear equations iteratively until the actual equations of motion are satisfied to a required tolerance.

The degenerated three-dimensional shell element is obtained from the three-dimensional solid element by imposing two constraints: 1) Straight lines normal to the midsurface before deformation remain straight but not normal after deformation; and 2) the transverse normal components of strain and hence stress are ignored in the development. The resulting nonlinear formulation admits arbitrarily large displacements

and rotations of the shell element and small strains, since the thickness does not change and the normal does not distort.

In the process of evaluating the integrals in Eq. (1), Gauss quadrature is used in the membrane directions of the shell, but explicit integration is used in the thickness direction (for elastic behavior). Thus, the thickness direction integration for all three matrices reduces to the following classical laminate stiffnesses:

$$[A] = \sum_{j=1}^{P} [C']_j(\zeta_{j+1} - \zeta_j)$$

$$[B] = \frac{1}{2}\sum_{j=1}^{P} [C']_j(\zeta_{j+1}^2 - \zeta_j^2) \qquad (2)$$

$$[D] = \frac{1}{3}\sum_{j=1}^{P} [C']_j(\zeta_{j+1}^3 - \zeta_j^3)$$

where ζ_j is the thickness direction lower coordinate of the jth lamina, P is the number of laminas, and $[C']$ is the orthotropic constitutive matrix for the jth lamina in the shell curvilinear body coordinates. It should be noted that $[C']$ is a function of the lamina properties E_{11}, E_{22}, ν_{12}, G_{13}, G_{23}, G_{12}, and the ply orientation angle.

Micromechanics Model

The Aboudi micromechanics model is included to study the effect of micromechanics constituent properties as random variables. In this section a review of Aboudi's theory is discussed, which is modeled after the development in Ref. 8.

This theory involves the solution of a suitable boundary value problem whose domain is a typical representative volume V. The composite is modeled as an isotropic matrix reinforced by a transversely isotropic fiber of rectangular cross section. The fibers extend in the x_1 direction and are arranged in a doubly periodic array in the x_2 and x_3 directions as shown in Fig. 1a. The rectangular fiber has cross-sectional dimensions h_1, ℓ_1 with h_2, ℓ_2 denoting the matrix spacing. Figure 1b shows the representative cell necessary for analysis due to the periodic arrangement. The cell is further divided into four subcells α, β, = 1, 2, each with a local coordinate system $(x_1, \bar{x}_2^{(\alpha)}, \bar{x}_3^{(\beta)})$.

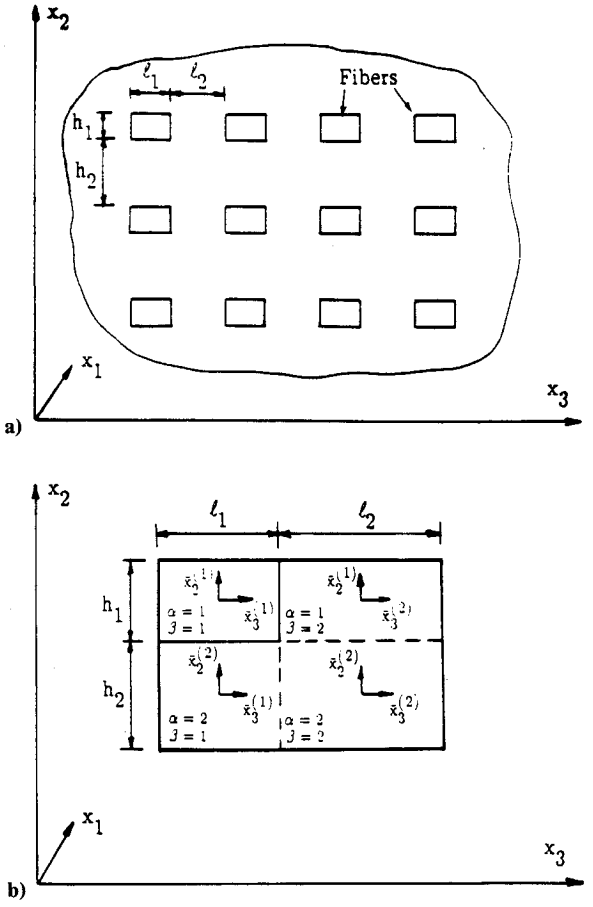

Fig. 1 Micromechanics subcell geometry: a) doubly periodic array of rectangular fibers extending in the x_1 direction; b) representative cell.

The displacement field considered by Aboudi is a first-order expansion in each subcell, since only average behavior of the composite is sought. This displacement field of Aboudi is given by

$$\Delta_i^{(\alpha\beta)} = w_i^{(\alpha\beta)} + \bar{x}_2^{(\alpha)}\phi_i^{(\alpha\beta)} + \bar{x}_3^{(\beta)}\psi_i^{(\alpha\beta)}, \qquad i = 1, 2, 3 \qquad (3)$$

where $w_i^{(\alpha\beta)}$ are the displacement components of the center of the subcell and $\phi_i^{(\alpha\beta)}$ and $\psi_i^{(\alpha\beta)}$ characterize the linear variations of the displacements within the subcell in the $\bar{x}_2^{(\alpha)}$ and $\bar{x}_3^{(\beta)}$ directions, respectively. In this section, repeated α and β do not imply summation.

By imposing the continuity conditions at the boundaries of the subcells, closed-form solutions for the average stress in the cell $\bar{\sigma}_{ij}$ in terms of the average strain $\bar{\epsilon}$ can be obtained. Without listing the details (see Ref. 8), the results are summarized by

$$\{\bar{\sigma}\} = [Q]\{\bar{\epsilon}\}$$

where the Q_{ij} are the effective elastic constants of the composite. The constants Q_{ij} are given in functional form as

$$Q_{ij} = f(C_{ij}^{(\alpha\beta)}, h_\alpha, \ell_\beta)$$

and $C_{ij}^{(\alpha\beta)}$ represent the constitutive properties of the $(\alpha\beta)$ subcell.

Probabilistic Finite Element Method

The second-moment perturbation method as developed by Liu et al.[4-6] is summarized in this section for geometric nonlinear, time-independent behavior. Discussions of importance to composite random variables are presented, and developments are applied to the degenerated three-dimensional shell element. The first-order reliability method incorporated into the computational scheme is also described.

Begin by rewriting the assembled form of Eq. (1) as

$$\{F(\{\Delta\},\{b\})\} = \{R(\{b\})\} \qquad (4)$$

where $\{F\}$ is the internal force vector, $\{\Delta\}$ the displacement vector, $\{R\}$ the external force, and $\{b\}$ a discretized vector of the random function $b(x)$, where x is a spatial coordinate $\{x\}$. As in typical finite element analysis, the random function $b(x)$ is expanded using shape functions $\psi_i(x)$:

$$b(x) = \sum_{i=1}^{n} \psi_i(x)b_i \qquad (5)$$

where b_i are the nodal values of $b(x)$. Generally the random quantity b can be a material property, geometric dimension, or a load.

The probabilistic finite element method for moment evaluation proceeds by applying second-moment analysis. The vectors in Eq. (4) are expanded about the mean of the random function b via Taylor series, and following substitution into Eq. (4) the following perturbation equations are obtained:

Zeroth-order equation:

$$\{\bar{F}\} = \{\bar{R}\} \qquad (6)$$

First-order equations:

$$[\bar{K}^T]\{\bar{\Delta}\}_{b_i} = \{\bar{R}\}_{b_i} - \{\bar{F}\}_{b_i}, \qquad i = 1, \ldots, n \qquad (7)$$

where the overbar represents evaluation of that term at the mean value of b, and the subscript b_i represents the derivative

with respect to b_i. It should be noted that, when the perturbation Eqs. (6) and (7) are used for reliability analysis, the overbar indicates evaluation about the "most probable failure point" in the optimization procedure. As is common in the literature, $[K^T]$ represents the tangent stiffness matrix defined as

$$[K^T] = \frac{\{\partial F\}}{\{\partial \Delta\}} \tag{8}$$

For linear elastic problems, the term $\{\bar{F}\}_{b_i}$ in Eq. (7) is in the following form:

$$\{\bar{F}\}_{b_i} = [\bar{K}]_{b_i}\{\bar{\Delta}\}$$

and for geometric nonlinear elastic problems, this term becomes

$$\{\bar{F}\}_{b_i} = \int_V [B_L]^T\{\hat{S}\}_{b_i}\, dV$$

Once $\{\bar{\Delta}\}$ and $\{\bar{\Delta}\}_{b_i}$ are obtained by solving Eqs. (6) and (7), the mean and autocovariance matrices for the nodal displacements can be determined. The first-order estimate of the mean displacement is given by [see Eq. (4)]:

$$E[\{\Delta\}] \cong \{\bar{\Delta}\} \tag{9}$$

where $E[\cdot]$ indicates the expected value or mean. Similarly, the first-order autocovariance of displacement is given by

$$\text{cov}(\Delta^r, \Delta^s) = \sum_{i,j=1}^{n} \bar{\Delta}^r_{b_i}\bar{\Delta}^s_{b_j}\,\text{cov}(b_i, b_j) \tag{10}$$

where $\text{cov}(b_i, b_j)$ is the covariance of the random function b. It is defined in terms of the input coefficient of variation α and the autocorrelation coefficient function $A[b(x_i), b(x_j)]$. The actual autocorrelation function selected will be discussed later. The covariance $\text{cov}(b_i, b_j)$ is given by

$$\text{cov}(b_i, b_j) = \{\text{var}[b(x_i)]\text{var}[b(x_j)]\}^{1/2} A[b(x_i)b(x_j)] \tag{11a}$$

where

$$\text{var}[b(x_i)] = \alpha^2 E[b(x_i)]^2 \tag{11b}$$

Similar procedures are used to evaluate statistical moments of the stress response.

Composite Random Variables

Sources of randomness can be material properties, geometric dimensions, or loads. For the present study, the only geometric dimensions selected as random variables are the ply thickness and ply angle. The loading is considered to be deterministic throughout this study. All material properties are treated as random variables, either from the point of view of the ply level or the micro level (when the micromechanics constitutive theory is incorporated). At the ply level, material variables could be any of the engineering material properties E_{11}, E_{22}, ν_{12}, G_{12}, G_{13}, G_{23}. Recall that these properties along with the ply angle θ define the coefficients of the constitutive matrix $[C']$. At the micromechanics level, the material variables could be the fiber and matrix properties E_{f11}, E_{f22}, G_{f12}, ν_{f12}, ν_{f23}, E_m, ν_m, FVR, where f denotes fiber property, m denotes a matrix property, and FVR is the fiber volume ratio. These microvariables are used in the Aboudi micromechanics equations to determine the engineering (ply-level) material properties. In this section, discussions involving the technical assumptions and subtleties of incorporating these random variables are presented.

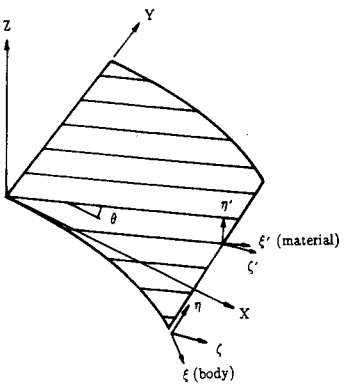

Fig. 2 Body and material coordinates in the shell curvilinear plane.

Ply Thickness

The total thickness of a laminate is determined by summing the individual ply thicknesses, which for a composite made of one material type are assumed to be constant for every ply. Here it is assumed that the thickness of all layers fluctuate, but that the total thickness of the laminate (shell) remains unchanged. This is the assumption made by Nakagiri et al.[2] for eigenvalue analysis of composite plates. In Ref. 2 only ply thickness and orientation angle were selected as random variables. Since the total thickness is assumed to be constant, the ζ coordinates of the upper and lower surfaces of the shell are deterministic.

Micro-Level Material Properties

The micro-level random variables E_{f11}, E_{f22}, G_{f12}, ν_{f12}, ν_{f23}, E_m, ν_m, and FVR are specified inputs to the Aboudi micromechanics equations with the output being the ply-level engineering constants. These engineering constants are used to calculate the $[A]$, $[B]$, and $[D]$ matrix stiffnesses in Eqs. (2). Thus, to evaluate the $\{\bar{F}\}_{b_i}$ matrices needed in Eq. (7), Eqs. (2) must be differentiated in terms of the micro-level random variables. In this process, the chain rule of differentiation and the finite difference method (for differentiating the micromechanics equations) are utilized.[9]

Spatial Correlation

The probabilistic finite element procedure developed herein has the ability to model the correlation involved in spatial fields. For an orthotropic ply, and referring to Fig. 2, we assume an orthotropic autocorrelation coefficient function in the following form:

$$A(b_i, b_j) = \exp\left[-\left(\frac{\xi_i' - \xi_j'}{\lambda_{\xi'}}\right)^2\right]\exp\left[-\left(\frac{\eta_i' - \eta_j'}{\lambda_{\eta'}}\right)^2\right]$$
$$i, j = 1, \ldots, n \tag{12}$$

In Fig. 2, ξ and η are the curvilinear coordinates of the shell that are aligned with the body coordinates; ξ' and η' are the curvilinear coordinates in the principal material coordinate system, aligned with the fibers; and $\lambda_{\xi'}$, $\lambda_{\eta'}$ are input correlation lengths. Transforming ξ and η to the principal material coordinates ξ' and η', we obtain

$$\begin{Bmatrix}(\xi_i' - \xi_j')\\(\eta_i' - \eta_j')\end{Bmatrix} = \begin{bmatrix}\cos\theta & \sin\theta\\ -\sin\theta & \cos\theta\end{bmatrix}\begin{Bmatrix}(\xi_i - \xi_j)\\(\eta_i - \eta_j)\end{Bmatrix} \tag{13}$$

This formulation for the autocorrelation allows ply random variables to be correlated in the plane of the shell aligned with the material coordinates. For the case of material properties, we assume that they will have correlation trends that are parallel and perpendicular to the fiber directions.

An underlying assumption in Eq. (12) is that $A(b_i, b_j)$ is not a function of the shell thickness coordinate ζ. This leads to independent random fields from ply to ply (uncorrelated). This assumption is not a requirement, and correlation could

be assumed in the ζ direction, but for all of the examples given in this work all layers have been chosen to be independent.

Computational Savings Techniques

Three methods are utilized in this work to reduce the computational effort involved when a spatially correlated random field is assumed. Liu et al.[4-6] discussed techniques for diagonalizing the covariance matrix and an adjoint method for computing only the kth component of the displacement derivatives. Both of these are incorporated here, as well as a way to reduce the assembly time for stiffness and residual force derivatives by using the chain rule of differentiation.[9]

Reliability Estimation

Probability of failure estimation or reliability is a very important aspect of the computational procedure. The method used here is the first-order reliability method developed by Hasofer and Lind[10] and extended by Rackwitz and Fiessler.[11] Let $g(U_i) = 0$ be the limit state function in which U_i are the independent (uncorrelated) random variables. Each U_i is transformed to a reduced coordinate u_i according to

$$u_i = \frac{U_i - \mu_i}{\sigma_i} \tag{14}$$

where (μ_i, σ_i) are the mean and standard deviation, respectively, of U_i. Equation (14) is then substituted into $g(U_i)$ so that the limit state function is now expressed in terms of the reduced coordinates $g_1(u_i)$. The generalized safety index β is defined as the minimum distance from the origin of the reduced coordinates to the limit state surface. Thus, in mathematical terms the problem becomes the following constrained minimization problem:

$$\beta = \min\sqrt{\Sigma u_i^2}$$

$$\text{subject to} \qquad g_1(u_i) = 0 \tag{15}$$

Various optimization schemes are used to solve this problem; the one chosen here is a Lagrangian multiplier method.[12] The probability of failure P_f is then approximated from the standard normal cumulative distribution tables (ϕ) as

$$P_f = \phi(-\beta)$$

If $g(U_i)$ is linear in U_i and all U_i are normal, then P_f is exact. Otherwise P_f is an approximation.

Table 1 Material properties and statistics for graphite-epoxy spherical shell problem

Random variable	Mean	Standard deviation	Coefficient of variation	$\lambda_{\xi'}$	$\lambda_{\eta'}$
E_{11}	109.0	5.45	0.05	635	381
E_{22}	6.27	0.314	0.05	381	635
G_{12}	3.09	0.155	0.05	508	508
ν_{12}	0.222	1.112×10^{-2}	0.05	508	508
G_{13}	3.09	0.155	0.05	508	508
G_{23}	2.41	0.121	0.05	508	508
E_{f11}	2.14	10.7	0.05	635	381
E_{f22}	13.8	0.690	0.05	381	635
G_{f12}	13.8	0.690	0.05	508	508
ν_{f12}	0.2	1.0×10^{-2}	0.05	508	508
ν_{f23}	0.25	1.25×10^{-2}	0.05	508	508
E_m	3.45	0.173	0.05	635	635
ν_m	0.25	1.25×10^{-2}	0.05	635	635
FVR	0.5	2.5×10^{-2}	0.05	508	508
θ^a	0 deg, 90 deg	2 deg	—	635	635
δ^a	12.7	0.636	0.05	635	635

[a]θ Indicates fiber orientation angle; δ indicates ply thickness. Subscripts f and m represent fiber and matrix, respectively; absence of a letter subscript indicates a ply-level property. The units are GPa and mm where appropriate.

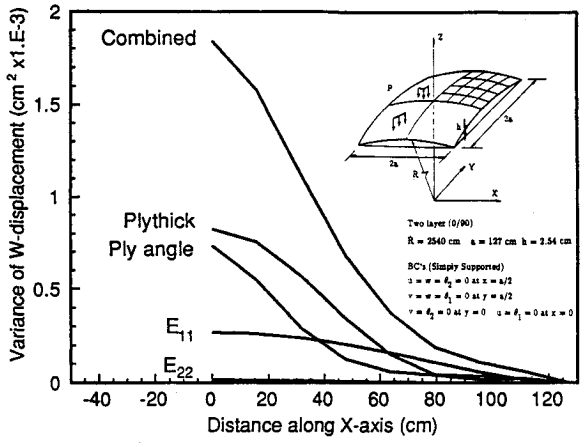

Fig. 3 Variance of center displacement w along x axis of spherical shell showing the combined and individual effects of the ply-level graphite-epoxy random variables.

Extensions to the aforementioned basic method have been developed by Rackwitz and Fiessler,[11] Chen and Lind,[13] and Wu and Wirsching[14]; these extensions provide improvements to the estimate of P_f. These improvements allow for other distributions than the normal (using equivalent normal distributions) and increased accuracy for nonlinear limit state functions.

In the process of solving the constrained minimization problem, derivatives of the limit state function with respect to the random variables are required. Since the limit state function is typically a function of the structural response (e.g., displacement, strain, and stress), then by the chain rule of differentiation, derivatives of the response with respect to the random variables are needed:

$$\frac{\partial g}{\partial U_i} = \frac{\partial g}{\partial \{\sigma\}} \frac{\partial \{\sigma\}}{\partial U_i} \tag{16}$$

where $\{\sigma\}$ denotes the stress vector. Since the derivatives $\partial\{\sigma\}/\partial U_i$ are already determined in the perturbation probabilistic finite element method, they can be used here to compute reliability. In this way an efficient procedure for reliability estimation incorporating the probabilistic finite element method is achieved.

Applications

Spherical Shell Under External Pressure

A shallow spherical shell with simply supported boundary conditions and uniform external pressure is studied in this example. The problem description is given in Fig. 3, and all input material properties, variances, and levels of spatial correlation are given in Table 1. The coefficient of variation (COV) is defined as the ratio of the standard deviation to the mean for a given random variable. All examples in this study used a COV of 0.05, except for the case of ply orientation angle, where the standard deviation was chosen to be 2 deg. All variables were treated as random fields, with typical correlation lengths of one-half of the domain of the problem in each principal material direction. Only one quadrant of the shell was modeled in the interest of computational savings, even though the spatial correlation assumptions may not be symmetric across the shell. Of course, this is not a limitation of the procedures or computational model developed herein.

The use of the probabilistic finite element procedure employed here for random fields requires that a convergence study be performed. Not only must the mesh be a reasonable one to discretize the deterministic equilibrium equations, but it also must be refined enough to discretize the chosen random field. Generally, as the correlation lengths are increased, the effect on mesh requirements is that a coarser mesh can be

used. In Ref. 9, this study was performed by comparing the second-moment results to the Monte Carlo method results. This led to the use of a 4×4 mesh of nine-node Lagrangian elements, with fully reduced (2×2) integration. The requirements of the random field proved to be the dominating factor in specifying this 4×4 mesh.

One important benefit of the probabilistic finite element method is the ability to quantify the variations in the structural response caused by individual random fields or variables. In the present study these random variables can include ply-level material stiffnesses or micro-level material stiffnesses. Figure 3 illustrates both the combined and individual variances for displacement response. It is interesting to note that, for this particular shell problem, the w-displacement response is most affected by the ply thickness, ply angle, and E_{11} variables. In Fig. 4 micromechanics-level random variables were chosen. For the w-displacement variance, once again ply thickness and ply angle were important, along with FVR and E_{f11} microvariables. It has been found that, for these shell problems with graphite-epoxy materials, generally the dominant random variable is the ply angle (especially for stress response), as would be expected due to the low stiffness of the matrix in comparison with the fibers.

A postbuckling analysis of the graphite-epoxy shell is performed next. The modified Riks method[15] is used to trace the nonlinear path past the snap-through point (or limit point) and into the postbuckling range. In Ref. 9, in order to validate the second-moment method for geometric nonlinear behavior, the second-moment results for the nonlinear buckling of this shell were compared to the Monte Carlo method with reasonably good agreement.

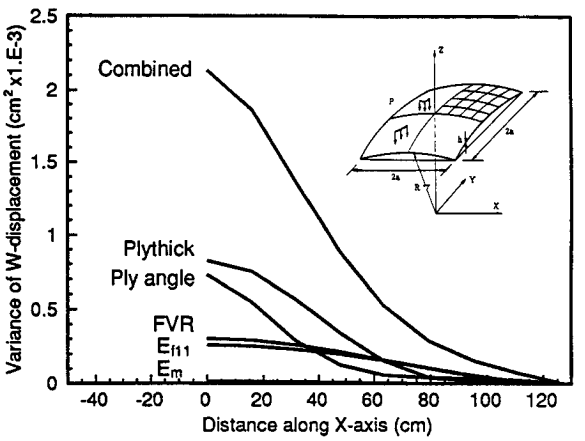

Fig. 4 Variance of center displacement w along x axis of spherical shell showing the combined and individual effects of the micro-level graphite-epoxy random variables.

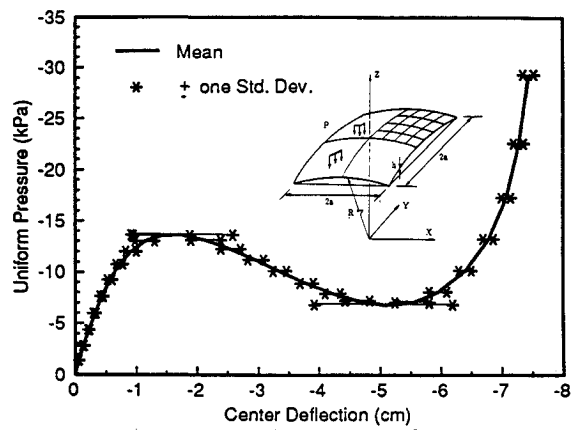

Fig. 5 Mean center displacement w and ± 1 standard deviation point vs load throughout postbuckling range of spherical shell.

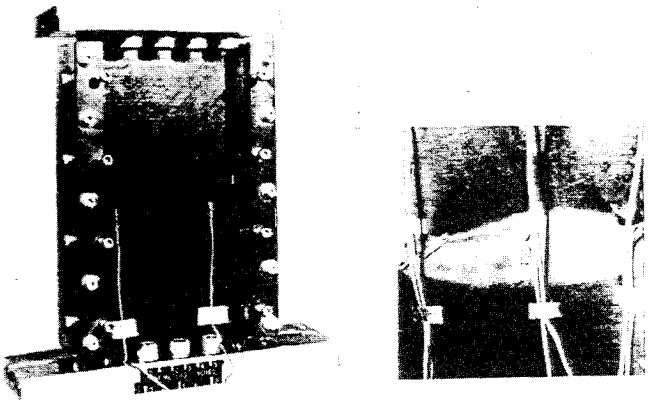

Fig. 6 Flat rectangular graphite-epoxy panel under axial compression[16]: a) panel fixture; b) panel failure mode.

Using the first-order second-moment method combined with the modified Riks technique, the w-displacement response throughout the postbuckling range, including the limit points, is calculated and presented in Fig. 5. Here the squares indicate mean response, and the asterisks are the mean ± 1 standard deviation (1σ) points. It is evident that at the limit points the COV is very large, in fact reaching a value of 0.5.

The increase in variance at the limit points occurs since the buckling behavior of the structure is more sensitive to any changes in stiffness or load at these points. It should be noted that, although the displacement COV begins at about 0.05 before the limit points, it becomes quite small after the limit points, settling to a value of about 0.01.

Postbuckling of a Flat Panel Under Axial Compression

The problem under consideration here is a flat, rectangular, 50.8-cm-long $\times$ 17.8-cm-wide graphite-epoxy panel loaded in axial compression. An experimental study was performed on a series of these panels by Starnes and Rouse.[16] Figure 6 shows a typical panel with fixture and the resulting failure mode. The loaded ends of the panels were clamped by fixtures and the unloaded edges were simply supported by knife-edge restraints to prevent the panels from buckling as wide columns. The material properties, layup, and statistics are as follows: $E_{11} = 131.0$ GPa (19,000 ksi), $E_{22} = 13.0$ GPa (1890 ksi), $G_{12} = G_{13} = 6.4$ GPa (930 ksi), $\nu_{12} = 0.38$, $G_{23} = 1.72$ GPa (250 ksi), and lamina thickness = 0.14 mm (0.0055 in.); the layup was a 24-ply orthotropic laminate with a $[\pm 45/0_2/\pm 45/0_2/\pm 45/0/90]_S$ stacking sequence; the random variables were: E_{11}, E_{22}, $G_{12}\nu_{12}$, G_{13}, G_{23}, and ply thickness, each with a coefficient variation of 0.05, also ply angle, with a standard deviation of 2 deg. The model used 72 nine-node Lagrange elements uniformly spaced, with 12 along the longitudinal (x direction) and 6 along the width (y direction), with 325 nodes and 1625 degrees of freedom. The boundary conditions are shown in the insert in Fig. 7.

We performed a previous deterministic analytical study on the panel (denoted panel C4 in Ref. 16); our results are given in Ref. 17. Comparisons were made between analytical and experimental results. In general the comparisons were very good, even deep in the postbuckling range. To pass the critical buckling load, a geometric imperfection of a small percentage of the plate thickness (typically 1–5 times the normal buckling mode) was added to the original geometry of the panel. The purpose of the previous analysis was to study the effect of shear deformation on postbuckling response and failure prediction. The purpose of this analysis is to study the variability of the panel results.

The probabilistic analysis of this panel assumed a fully correlated random field for each random function in each layer so that each degenerated to a single random variable per layer (this is referred to here as the uniform variance assump-

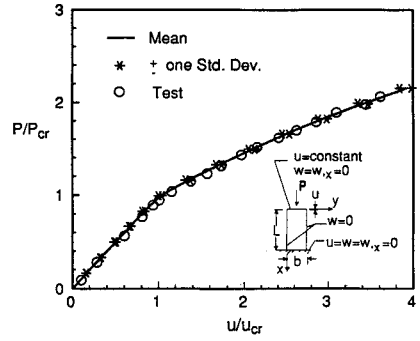

Fig. 7 End-shortening postbuckling response of graphite-epoxy panel.

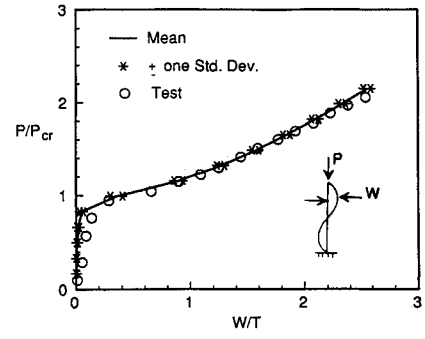

Fig. 8 Out-of-plane displacement postbuckling response of graphite-epoxy panel.

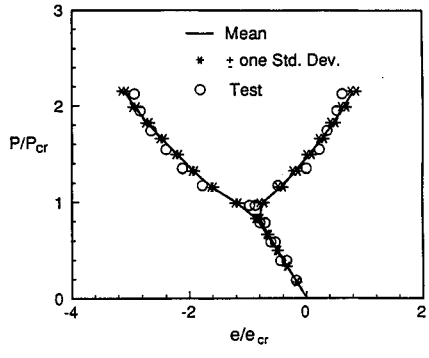

Fig. 9 Longitudinal surface strains on opposite outer surfaces of the graphite-epoxy panel near a point of maximum out-of-plane displacement.

tion). An attempt was made to employ the random field techniques; however, the computational expense was too high due to eight random fields in 24 layers, 1625 degrees of freedom in the model, and a nonlinear analysis. The random field method took 8.3 h/load step (on a Convex computer), whereas the uniform variance method only 5.8 min/load step. Since 13 load steps were required to reach the failure load and immense storage is required for the random field method with this many layers, it was concluded that for this size problem the uniform variance assumption was much more realistic.

The end shortening postbuckling response is shown here in Fig. 7. The load P is normalized by the analytical buckling load P_{cr} and the end shortening deflection u by the analytical end shortening u_{cr} at buckling. A 1% plate thickness geometric imperfection was used. The analytical results compare favorably with the experimental results. In addition, the ± 1 standard deviation points indicate the variation in the data. It should be noted that in Ref. 17 it was shown that one of the reasons for the good agreement here is the inclusion of the shear deformation in the element formulation. Figure 8 contains the out-of-plane deflection w near a point of maximum deflection normalized by the panel thickness t. Figure 9 shows the longitudinal surface strains e near a point of maximum out-of-plane deflection normalized by the analytical buckling strain e_{cr}. For all three of these plots the COV is typically around 2%, except for the w displacement prior to and at buckling, which was large.

To understand the failure mode, it is necessary to see the nonlinear buckling mode shape. An analytical contour plot of the out-of-plane deflection at an applied load of $2.1P_{cr}$ is shown in Fig. 10a. A moiré fringe pattern photograph from Ref. 16 of the out-of-plane deflections at the same load is shown in Fig. 10b. Both patterns indicate two longitudinal half-waves with a buckling mode nodal line at panel midlength.

In Refs. 16 and 17, it was determined that the failure mode was primarily due to transverse shear stress τ_{13} (τ_{xz} in 0-deg ply) along the midlength (nodal line) of the panel. Other stresses such as σ_{11} and τ_{12} also contribute to failure along the nodal line region in other layers.

The distribution of the transverse shear stress τ_{13} in the third layer of the laminate (a 0-deg ply) is shown in Fig. 11a for a load of $2.1P_{cr}$. It is observed that high transverse shear stress develops along the nodal line of the panel. Figure 11b shows the redistribution of the τ_{13} stress for three different applied loads. At the experimental failure load of $2.1P_{cr}$, the τ_{13} stress approaches the material allowable value of 62 MPa (9 ksi). The COV for the τ_{13} stress was typically 0.055 except at the critical buckling load, when it reached a value of 0.12.

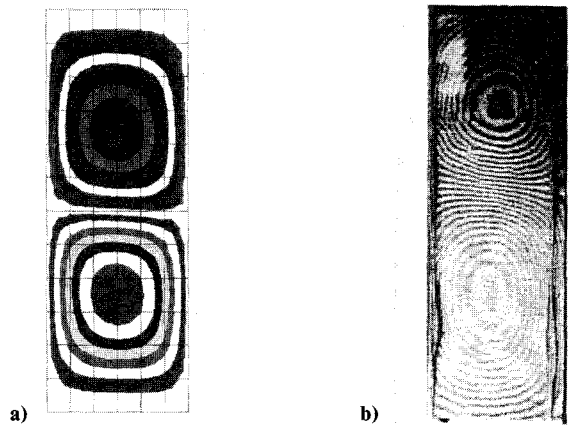

Fig. 10 Comparison of experimental and analytical out-of-plane displacement patterns at applied load of 2.1 P_{cr} for the graphite-epoxy panel: a) contour plot of analytical results; b) photograph of moiré-fringe pattern.

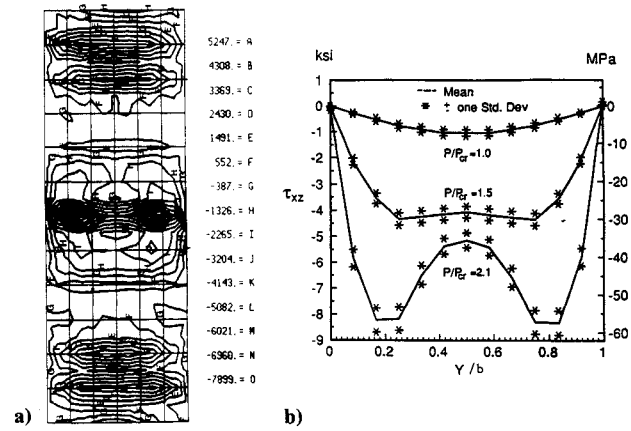

Fig. 11 Transverse shear stress τ_{xz} distributions in the third layer (0-deg ply) from the surface of the graphite-epoxy panel: a) contour plot of transverse shear stress distribution; b) stress distributions across panel midlength.

It is of interest to determine the most significant random variables in the variance for the τ_{13} stress. Figure 12 contains the peak mean τ_{13} stress, along with the COV for the combined and individual random variables for increasing load values. It is observed that the τ_{13} stress variance is most influenced by G_{13}, with the ply thickness effect increasing as the buckling load is passed and bending effects become more important.

Even though for this graphite-epoxy composite panel a first-ply failure does not represent overall panel failure, a reliability analysis was performed for first ply failure. In Ref. 17, it was shown that, although the failure mechanism was primarily due to τ_{13} transverse shear stress, the Tsai-Wu failure criterion that accounts for interaction of stresses did a better job of predicting failure than the maximum stress criterion. The Tsai-Wu criterion was thus selected as the limit state function for this example. Of course, the maximum stress, maximum strain, or other criteria could be used. The Tsai-Wu criterion can be stated as follows:

$$g = 1 - (F_1\sigma_1 + F_2\sigma_2 + 2F_{12}\sigma_1\sigma_2 + F_{11}\sigma_1^2 + F_{22}\sigma_2^2 + F_{44}\sigma_4^2 + F_{55}\sigma_5^2 + F_{66}\sigma_6^2) = 0$$

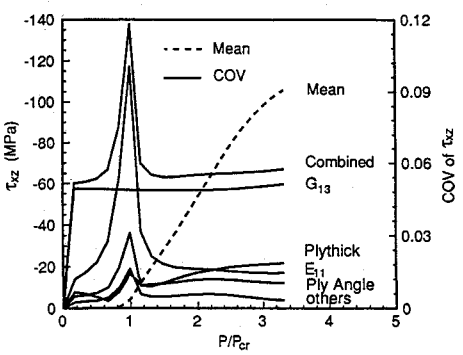

Fig. 12 Mean and COV of τ_{xz} stress vs load throughout postbuckling range showing the combined and individual effects of the ply-level random variables for the graphite-epoxy panel.

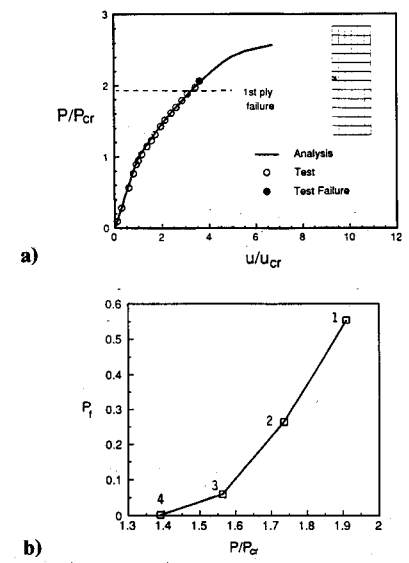

Fig. 13 First-ply Tsai-Wu deterministic failure and reliability analysis: a) end-shortening postbuckling response of panel showing deterministic Tsai-Wu first-ply failure; b) probability of first-ply failure P_f using the Tsai-Wu criterion.

where

$$F_1 = \frac{1}{X_t - X_c}; \quad F_2 = \frac{1}{Y_t - Y_c}; \quad F_{11} = \frac{1}{X_t X_c}$$

$$F_{22} = \frac{1}{Y_t Y_c}; \quad F_{44} = \frac{1}{R^2}; \quad F_{55} = \frac{1}{S^2}; \quad F_{66} = \frac{1}{T^2}$$

$$F_{12} = -\frac{1}{2}\sqrt{\frac{1}{X_t X_c Y_t Y_c}}$$

and σ_1 and σ_2 are the normal stresses along the fiber and normal to the fiber, respectively; σ_4, σ_5, and σ_6 are the shear stresses in the 23, 13, and 12 planes, respectively; X and Y correspond to strengths in the 1 and 2 directions, respectively; the subscripts t and c denote tension and compression, respectively; and R, S, and T are the shear strengths. The values of the strengths used are as follows: X_t = 1400 MPa (203 ksi), X_c = 1138 MPa (165 ksi), Y_t = 80.9 MPa (11.7 ksi), Y_c = 189 MPa (27.4 ksi), $R = S$ = 62 MPa (9 ksi), and T = 69.0 MPa (10.0 ksi).

All random variables were assumed to have normal distributions in this example reliability analysis. Since no experimental distribution data were available, then this "normal" assumption was used to reduce the reliability computation time in the optimization routine. Since no equivalent normal approximations were made, the number of iterations in the optimization routine was reduced (each iteration involves a complete new solution of the nonlinear finite element problem). Whereas all stiffness random variables were given a COV of 0.05, the strengths were assumed to have COV values of 0.10. In addition, zero correlation was assumed between each random variable. Of course, none of these simplifications are limitations of the method.

Figure 13a shows the deterministic comparison of the Tsai-Wu analytical prediction of first ply failure to the experimental failure. The failure location is indicated by an "x" in the insert and the thickness location is the first layer of the laminate. Figure 13b contains the reliability analysis. The probability of failure P_f was found to be quite small (0.0021) at the load P/P_{cr} = 1.39, which is still quite deep in the postbuckling range. The number of iterations for each numbered data point in Fig. 13b is as follows: point 1→5 iterations, point 2→6 iterations, point 3→8 iterations. The numerical tolerance for convergence in the reliability index β was set to 0.001. In terms of CPU time (on a Convex computer), the following expenditures were required for each data point: point 1→1.59 h, point 2→1.75 h, point 3→2.05 h.

Summary and Conclusions

A nonlinear probabilistic finite element analysis procedure for laminated composite shells is developed, and applications were investigated to numerically study the procedures. The first-order second-moment method for probabilistic finite element analysis of random fields was employed, and accuracy assessments based on comparisons with the Monte Carlo method were referred to in Ref. 9. The method was found to be quite accurate for small input coefficients of variation. A postbuckling example of a spherical shell was studied to investigate the variability of the shell beyond the limit points. A second postbuckling application (a flat panel in compression) involving many degrees of freedom and layers was studied to test the ability of the probabilistic method to deal with larger models. The random field techniques became far too costly, from both computational and storage viewpoints. The random fields were assumed to be fully correlated (or single random variables) to alleviate this problem. CPU expenditures in the reliability analysis were reported to provide information regarding the costs of the procedures, and comparisons with experimental data were included.

The degenerated three-dimensional laminated composite shell element proved to be accurate in modeling the geometric

nonlinear behavior of the postbuckled panel. The inclusion of transverse shear deformation was found to be critical, especially in the postbuckling range. It was demonstrated that the modified Riks arc length method works quite well with the second-moment probabilistic method and allowed mean and variance calculations to be made beyond zero-slope limit points, which often exist in shell structures.

Acknowledgment

The support of this research by NASA Lewis Research Center through Grant NAG-3-933 is gratefully acknowledged.

References

[1]Hisada, T., and Nakagiri, S., "Stochastic Finite Element Method Developed for Structural Safety and Reliability," *Proceedings of ICOSSAR '81, Third International Conference on Structural Safety and Reliability,* The Univ. of Trondheim, Trondheim, Norway, 1981, pp. 395–408.

[2]Nakagiri, S., Takabatake, H., and Tani, S., "Uncertain Eigenvalue Analysis of Composite Laminated Plates by the Stochastic Finite Element Method," *Journal of Engineering for Industry,* Vol. 109, No. 1, Feb. 1987, pp. 9–12.

[3]Tani, S., and Nakagiri, S., "Reliability Synthesis of CFRP Laminated Plate," *Proceedings of ICOSSAR '89 Fifth International Conference on Structural Safety and Reliability,* San Francisco, CA, 1989, pp. 2079–2082.

[4]Liu, W. K., Belytschko, T., and Mani, A., "Random Field Finite Elements," *International Journal for Numerical Methods in Engineering,* Vol. 23, No. 10, 1986, pp. 1831–1845.

[5]Liu, W. K., Belytschko, T., and Mani, A., "Probabilistic Finite Elements for Nonlinear Structural Dynamics," *Computer Methods in Applied Mechanics and Engineering,* Vol. 56, No. 1, 1986, pp. 61–81.

[6]Liu, W. K., Mani, A., and Belytschko, T., "Finite Element Methods in Probabilistic Mechanics," *Probabilistic Engineering Mechanics,* Vol. 2, No. 4, 1987, p. 201.

[7]Chao, W. C., and Reddy, J. N., "Analysis of Laminated Composite Shells Using a Degenerated 3-D Element," *International Journal for Numerical Methods in Engineering,* Vol. 20, No. 11, 1984, pp. 1991–2007.

[8]Aboudi, J., "Closed Form Constitutive Equations for Metal Matrix Composites," *International Journal Engineering Science,* Vol. 25, No. 9, 1987, pp. 1229–1240.

[9]Engelstad, S. P., "Nonlinear Probabilistic Finite Element Modeling of Composite Shells," Ph.D. Dissertation, Engineering Science and Mechanics Dept., Virginia Polytechnic Institute and State Univ., Blacksburg, VA, Dec. 1990.

[10]Hasofer, A. M., and Lind, N. C., "Exact and Invariant Second-Moment Code Format," *ASCE Journal of the Engineering Mechanics Division,* Vol. 100, No. EM1, Feb. 1974, pp. 111–121.

[11]Rackwitz, R., and Fiessler, B., "Structural Reliability Under Combined Random Load Sequences," *Computers and Structures,* Vol. 9, No. 5, 1978, pp. 489–494.

[12]Ang, A. H. S., and Tang, W. K., *Probability Concepts in Engineering Planning and Design: Basic Principles,* Vols. 1 and 2, Wiley, New York, 1984.

[13]Chen, X., and Lind, N. C., "Fast Probability Integration by Three Parameter Normal Tail Approximation," *Structural Safety,* Vol. 1, No. 4, 1983, pp. 169–276.

[14]Wu, Y.-T., and Wirsching, P. H., "A New Algorithm for Structural Reliability Estimation," *ASCE Journal of Engineering Mechanics,* Vol. 113, No. 9, 1987, pp. 1319–1336.

[15]Crisfield, M. A., "A Fast Incremental/Iterative Solution Procedure that Handles 'Snap-Through'," *Computers and Structures,* Vol. 13, Nos. 1–3, 1980, pp. 55–62.

[16]Starnes, J. H., Jr., and Rouse, M., "Postbuckling and Failure Characteristics of Selected Flat Rectangular Graphite-Epoxy Plates Loaded in Compression," AIAA Paper 81-0543, April 1981.

[17]Engelstad, S. P., Knight, N. F., Jr., and Reddy, J. N., "Postbuckling Response and Failure Prediction of Flat Rectangular Graphite-Epoxy Plates Loaded in Axial Compression," AIAA Paper 91-0910-CP, April 1991.